RESEARCH ARTICLE

Editorial Process: Submission:10/13/2022 Acceptance:03/11/2023

Digital Breast Tomosynthesis: Three-Dimensional Measurement of Breast-Absorbed Dose Distribution

Erika Nakajima*, Hitoshi Sato

Abstract

Background: The dose exposure associated with digital breast tomosynthesis (DBT) is evaluated by multiplying the mean glandular dose (MGD) of mammography (MMG) with the correction coefficient of the angle of X-ray incidence. However, it has been pointed out that there are various problems when using the MGD as a standard for risk assessment in breast cancer screening. Therefore, the aim of this study was to assess the breast-absorbed dose for different breast sizes for dose assessment. Furthermore, in this study, by measuring the dose distribution three-dimensionally, we aimed to examine the MGD correction method using the breast size as a factor. **Methods:** A simulated breast phantom with a diameter of 40–160 mm and a total thickness of 40 mm, made with polymethyl methacrylate, was created by simulating the phantom shape used in the simulation calculation for calculating the MGD. It was made with polymethyl methacrylate. Radiochromic films were placed at different depths, which measured the breast-absorbed dose distribution three-dimensionally. The MGD was calculated from the breast-absorbed dose distribution obtained. **Results:** The three-dimensional dose distribution revealed that there was a difference in the distribution of MMG and DBT with increasing depth. In addition, a lower X-ray energy and a smaller breast size resulted in a greater difference in the absorbed dose between DBT and MMG. **Conclusion:** Incorporating the DBT correction according to the breast size into the MGD improves the accuracy of dose evaluation by the MGD. Additionally, a corrected MGD provides useful information for risk assessment when DBT is used for breast cancer screening.

Keywords: Digital breast tomosynthesis- breast dose distribution- MGD- radiochromic film

Asian Pac J Cancer Prev, **24 (3)**, 953-960

Introduction

Currently, mammography (MMG) has been scientifically proven to be an effective technique for breast cancer screening. The greatest advantage of breast cancer screening is the reduction of mortality via the early detection of breast cancer. In contrast, its disadvantages include radiation exposure, false-positive or negative diagnosis, over diagnosis, physical burden, and psychological burden. The effectiveness of the screening depends on a comprehensive judgment that considers the balance between the advantages and disadvantages (Sylvia et al., 2011).

In a dense breast, it is difficult to diagnose the presence of a tumor using MMG as MMG imaging overlaps with the mammary glands and tumors (Thomas et al., 2002). Therefore, MMG may be less effective for screening individuals with dense breasts, and other methods are needed to improve the sensitivity of breast cancer screening (Suzuki et al., 2021).

Digital breast tomosynthesis (DBT) is attracting attention as an additional function of the mammography system (Alakhras et al., 2013). In DBT, approximately 10 X-ray irradiations are performed using the step-and-shot method, and the projected images at each angle are collected (Uematsu, 2013). The use of DBT minimizes or eliminates the limitation of MMG associated with the mammary glands and mass overlap (Helvie, 2010; Sechopoulos, 2013). Therefore, this technique reduces the rate of false positives and false negatives. The use of DBT images has been reported to potentially improve the diagnosis and examination accuracy in individuals with dense breasts, reduce the requirement for re-examination, improve the conviction of interpretation, and identify the location of lesions (Helvie, 2010; Houssami and Skaane, 2013; Skaane et al., 2013; Gilbert et al., 2015; Chong et al., 2019; Kulkami et al., 2021; Mackenzie et al., 2021).

Irrespective of the effectiveness, radiation exposure is unavoidable for every individual undergoing breast cancer screening using X-rays. Therefore, it is necessary to consider the risk of radiation exposure (Ali et al., 2015).

Dance et al., (2011) proposed a method for estimating the mean glandular dose (MGD) of DBT using Eq. (1). This is a method of assessing the average absorbed dose

*Department of Radiological Sciences, Ibaraki Prefectural University of Health Sciences, Ibaraki Prefecture, Japan. *For Correspondence: nakajimae@ipu.ac.jp*

by the mammary glands in a compressed breast. MGD is simulated using a polymethyl methacrylate (PMMA) phantom with a diameter (symbol: φ) of 160 mm and a thickness of 40 mm as a substance simulating a standard breast (compression breast thickness, 45 mm; mammary gland/fat ratio, 41/59). The MGD is a product of air kerma (K), on the surface of the breast with coefficient factor g, corresponding to 50% of the mammary gland mass coefficient factor c, for correcting the difference in breast composition from 50% glandularity, and coefficient factor s for the target/filter combination. Additionally, it is calculated using a coefficient factor T that considers the effect of obliquely incident X-rays.

$$MGD = K \times g \times c \times s \times T \quad (1)$$

The MGD estimates the average of the breast-absorbed dose that changes depending on the subject's breast thickness and mammary gland concentration (Dance et al., 2011). In the case of MMG, the MGD evaluated using the PMMA phantom does not match the actual breast-absorbed dose (Dance et al., 2005; Sechopoulos et al., 2012; Hernandez et al., 2015; Wang et al., 2017; Sarno et al., 2018; Chang et al., 2020; Huda and Antar, 2020). In DBT cases, it has been reported that when the shape of the phantom is made closer to that of the actual breast, the peripheral part of the breast absorbs a higher dose than the central part at a depth of 20 mm from the surface (Flores et al., 2019). In addition, as X-rays are obliquely incident, there is an effect of scattered radiation from the compression plate and breast support. In particular, it has been reported that the contribution becomes more pronounced as the projection angle increases (Diaz et al., 2019). Therefore, the dose distribution in the breast is presumed to be complicated. Furthermore, the composition of the human breast has been elucidated using breast-dedicated CT, and the coefficient factor T increases when the dose is evaluated considering the breast model (Sarno et al., 2018).

In a previous study, to evaluate the validity of the MGD of DBT by Monte Carlo simulation, the two-dimensional dose distribution in the phantom was actually measured by inserting a radiochromic film (RCF) into the phantom for each depth (Sarno et al., 2017). However, the analyzed area included only three positions on the chest wall side and one position on the nipple side, but not the entire breast. In another study, the dose distribution by depth in the phantom was evaluated considering the shape of the breast. However the setting of the region of interest was limited only to the chest wall side and nipple side (Flores et al., 2019).

In accordance with the direction of X-ray incidence in DBT, the difference in breast size is considered to be related to the exposure dose. Currently, the evaluation of MGD is performed by simulating the breast size of European/US populations. The breast size is simulated using a PMMA phantom with a diameter (φ) of 160 mm and a thickness of 45 mm. However, the average breast diameter (φ) in Japanese women was reported to be 89.4 mm (National Institute of Bioscience and Human-Technology, 1996). To date, only a few studies have examined the exposure dose owing to the difference in breast size.

To evaluate the dose absorbed by the breast for dose evaluation and to examine the risks associated with the use of DBT for breast cancer screening, this study focused on breast size and changes in breast dose distribution associated with DBT. Furthermore, our aim was to examine the MGD correction method using breast size and X-ray energy as factors by measuring dose distribution three-dimensionally.

Materials and Methods

Study design

The PMMA phantom sizes used in this study were φ160 mm (Dance, 1990), which is the standard breast phantom size; φ80 mm, which is close to the average breast size of Japanese women; and φ40 mm, which is close to the clinically smallest size. The direction of and the direction perpendicular to the chest wall-nipple are described as directions Y and X, and the X-ray tube-breast support direction is described as direction Z. The origins of directions X and Y were the center of the incident X-ray and the edge of the chest wall, respectively; the origin of direction Z was 40 mm above the breast support. The size of the phantom in direction Y was half of that in direction X. The total thickness was 40 mm by combining 5-mm and 10-mm phantoms. A schematic diagram of the prepared phantom is shown in Figure 1. The RCFs were sized 170 mm × 85 mm, 90 mm × 45 mm, and 50 mm × 25 mm, for the phantom sizes of φ160 mm, 80 mm, and 40 mm, respectively. At depths of 0–10 mm and 20–40 mm from the surface of the phantom, RCFs were loaded at 5 mm and 10 mm intervals, respectively. There were six layers in total.

Dose evaluation using RCF

The type of RCF was XR-SP2 (lot#01212101; ASHLAND, Covington, KY, USA). The RCF used the background correction method to convert the *Δpixel* values into air kerma K (Saur and Frengen, 2008). For irradiation, we used Senographe Pristina (GE, Fairfield, CT, USA) equipment. The irradiation conditions were target/filter combination of Mo/Mo and tube voltage of 24–32 kV. Additionally, to simulate the actual human body, a 40-mm thick PMMA plate that simulates the pectoralis major muscle was placed by the phantom. Figure 2 shows the measurement layout figure and photo when the K in the phantom was measured using RCF. The phantom was placed at the center of the X-ray machine in direction X and fixed with a compression plate in direction Y such that it was in line with the edge of the chest wall. Furthermore, the average energy (E_{ave}) of incident X-ray at each depth was calculated using the simulation calculation software MoXS-5 (Molybdenum target X-ray Spectrum, ver.5). Using E_{ave}, we referred to the data of the National Institute of Standards and Technology to obtain the mass energy absorption coefficient ratio of air and phantom $\left(\frac{\mu_{en}}{\rho}\right)_{PMMA,air}$ (data by National Institute of Standards and Technology). The absorbed dose in the phantom for each depth (D_d) was calculated from Eq. (2).

$$D_d = K \times \left(\frac{\mu_{en}}{\rho}\right)_{PMMA,air} \quad (2)$$

Examination of correction coefficient of average absorbed dose

The average dose absorbed by the phantom ($\bar{D}_{all}$) measured using RCF was calculated from Eq. (3).

$$\bar{D}_{all} = \frac{1}{n}\sum_{1}^{n} \bar{D}_d \quad (3)$$

The ratio R_T of $\bar{D}_{all}$ with respect to MMG and DBT was calculated from Eq. (4).

$$R_T = \frac{\bar{D}_{all,DBT}}{\bar{D}_{all,MMG}} \quad (4)$$

Here, $\bar{D}_{all,DBT}$ indicated the average dose absorbed by the phantom subjected to DBT, and $\bar{D}_{all,MMG}$ indicated the average dose absorbed by the phantom subjected to MMG. Furthermore, the ratio of $\bar{D}_{all}$ because of the difference in the phantom size was calculated. The ratios f_{80} and f_{40} for phantoms of sizes φ80 mm and φ40 mm, respectively, were calculated from Eq. (5) and Eq. (6) with φ160 mm as the reference.

$$f_{80} = \frac{\bar{D}_{all,\varphi 80}}{\bar{D}_{all,\varphi 160}} \quad (5)$$

$$f_{40} = \frac{\bar{D}_{all,\varphi 40}}{\bar{D}_{all,\varphi 160}} \quad (6)$$

In Eq. (5), $\bar{D}_{all,\varphi 80}$ and $\bar{D}_{all,\varphi 160}$ indicated the average doses absorbed by the φ80-mm and φ160 mm phantoms. In Eq. (6), $\bar{D}_{all,\varphi 40}$ indicates the average dose absorbed by the φ40 mm phantom.

Results

Dose evaluation using RCF

The ratio of the mass energy absorption coefficient of air calculated from the X-ray spectrum to the mass energy absorption coefficient of PMMA ($(\frac{\mu_{en}}{\rho})_{PMMA,air}$) was approximately 0.62–0.63 regardless of the depth, Z. The absorbed dose, D_d, in the phantom in the XY direction of MMG and DBT with a tube voltage of 24 kV and φ40 mm is shown in the color map by depth (Figure 3a, b). In addition, regions that were 7 mm away from the edge of the chest wall were out of the irradiation field. In both cases, the dose decreased with an increase in the depth, Z. Moreover, with an increase in the depth, the dose at the phantom edge was higher for DBT than for MMG.

Figure 4 shows the color map of the dose absorbed D_d by the phantom on the XZ plane when the tube voltage was 24 kV and the phantom sizes were φ160 mm, 80 mm, and 40 mm. The smaller the phantom size, the greater the difference in the absorbed dose distribution with respect to MMG and DBT. Especially, at a deep position in direction Z, the DBT-associated dose at the edge was higher than the MMG-associated dose. This phenomenon became more remarkable with a decrease in tube voltage.

Table 1 shows the results of $\bar{D}_{all}$ obtained from Eq. (3). $\bar{D}_{all}$ was between 8.15 μGy/mAs and 26.2 μGy/mAs in MMG. In DBT, it was between 7.90 and 25.2 μGy/mAs. In both MMG and DBT, the higher the energy regardless of the phantom size, the higher the $\bar{D}_{all}$ in the phantom. With MMG, $\bar{D}_{all}$ was smaller for all tube voltages as the phantom size was smaller.

Table 1. Average Absorbed Dose by All Phantoms ($\bar{D}_{all}$).

Tube Voltage [kV]	φ [mm]	$\bar{D}_{all}$ [μGy/mAs]	
		MMG	DBT
24	160	8.97	8.83
	80	8.22	7.9
	40	8.15	9.5
28	160	16.9	17
	80	16.1	16.6
	40	15.3	16.8
32	160	26.2	25.2
	80	22.9	23.4
	40	23.4	24

DBT, digital breast tomosynthesis; MMG, mammography

Examination of correction coefficient of average absorbed dose

Using Eq. (4), the dose ratio R_T of $\bar{D}_{all}$ of DBT and MMG was calculated. The results are presented in Table 2. Concerning the phantom size, when the phantom size was small, the R_T increased. The largest R_T was 1.166 when the tube voltage was 24 kV and phantom size was φ40 mm. From Table 2, R_T values at the phantom size of φ160 mm were 0.985, 1.008, and 0.963 at tube voltages of 24, 28, and 32 kV, respectively, with an average of 0.985. Furthermore, the averages for the phantom sizes of φ80 mm and φ40 mm were 1.006 and 1.098, respectively.

Figure 5 shows f_{80} and f_{40} of $\bar{D}_{all}$ due to the difference in phantom size based on φ160 mm phantoms. It was 0.87–0.95 for both f_{80} and f_{40} regardless of the tube voltage for MMG. With respect to DBT, f_{80} was lower than 1 regardless of tube voltage, as in the case of MMG, and f_{40} was lower than 1 at tube voltages of 28 kV and 32 kV. Especially, $\bar{D}_{all}$ values at φ80 mm and φ40 mm were lower than that at φ160 mm. However, the f_{40} at a tube voltage of 24 kV was 1.08. The relational expression between f_{40} and tube voltage in DBT is presented in Eq. (7).

$$f_{40} = 0.0016x^2 - 0.1038x + 2.67 \quad (7)$$

In this equation, x indicates the tube voltage.

Table 2. Ratio R_T of $\bar{D}_{all}$ between DBT and MMG.

φ [mm]	Tube Voltage[kV]			mean
	24	28	32	
160	0.985	1.008	0.963	0.985
80	0.962	1.032	1.023	1.006
40	1.166	1.102	1.026	1.098

DBT, digital breast tomosynthesis; MMG, mammography

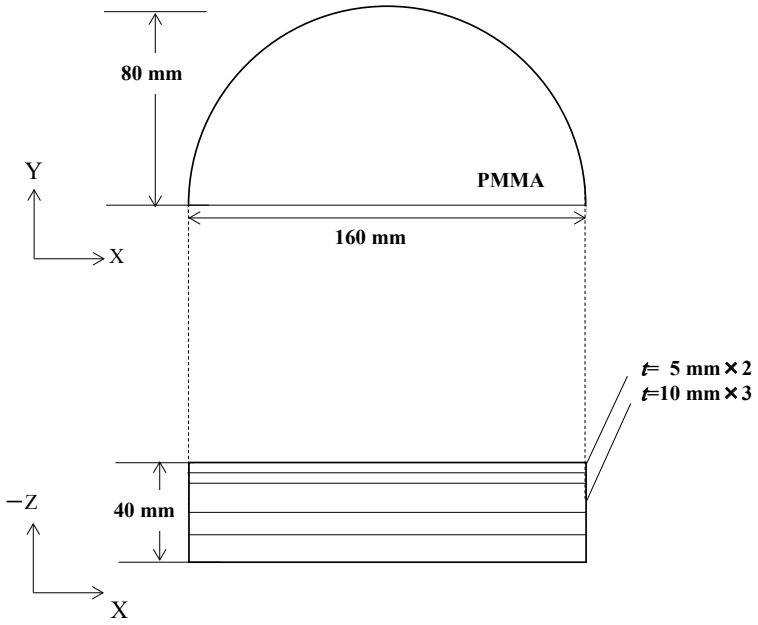

Figure 1. Semi-Cylindrical PMMA Phantom Diagram. PMMA, polymethyl methacrylate

Discussion

In this study, the dose distribution in the phantom of MMG and DBT was measured three-dimensionally using RCF. With the metal-oxide-semiconductor field effect transistor and thermoluminescent dosimeter used to measure the dose distribution in the phantom, the measurement location is limited to the representative points (Fedon et al., 2018). However, using the RCF, the dose distribution in the phantom was obtained with high spatial resolution. By using RCF, the dose distribution at the periphery of the phantom could be measured in detail.

Figure 3 shows that a deeper depth indicated the use of lower doses of MMG and DBT. The difference between MMG and DBT was noticeable at the edges. Especially when compared at a depth Z = 40 mm, it was visually confirmed that the dose at the margin was higher in DBT than in MMG. As shown in Figure 4, as the phantom size decreased, the absorbed dose D_d at the edge of the two-dimensional dose distribution of DBT tended to increase with respect to MMG. In particular, when comparing the two-dimensional distributions of absorbed dose D_d with a φ40 mm phantom, the dose distributions of MMG and DBT differed at the phantom edge, and the dose of DBT

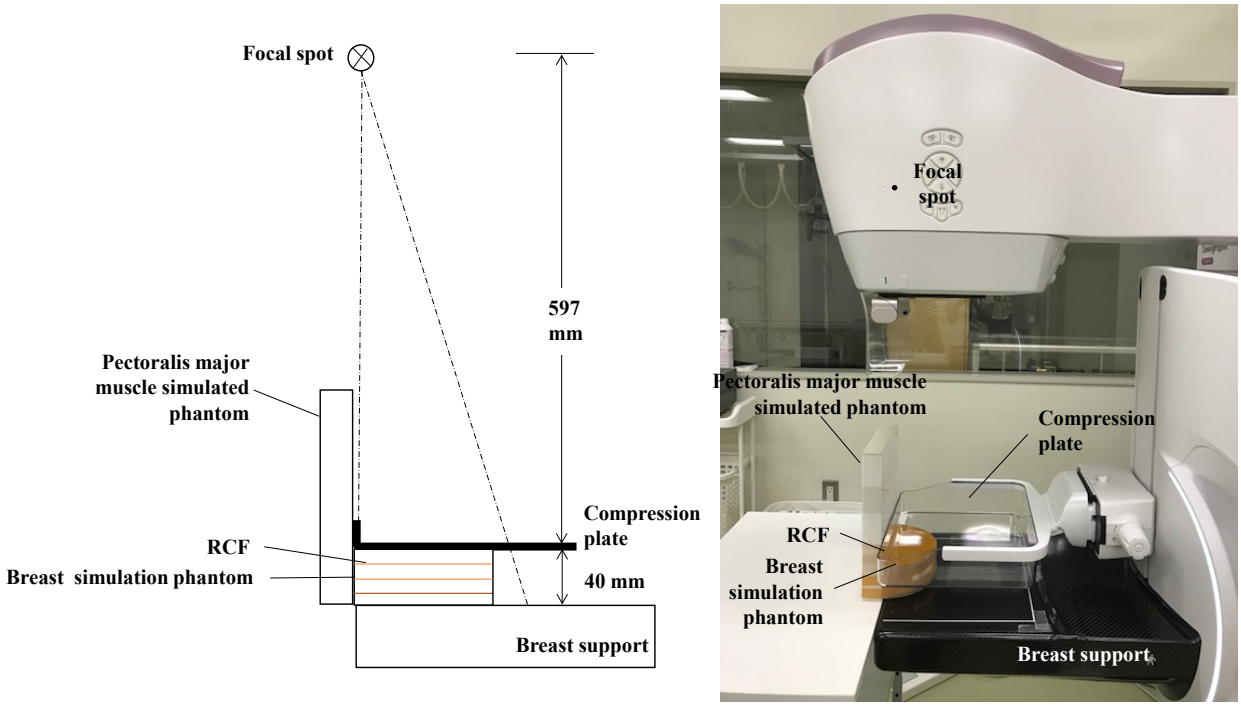

(a) figure (b) photo

Figure 2. Layout for the Measurement of K in the Phantom.

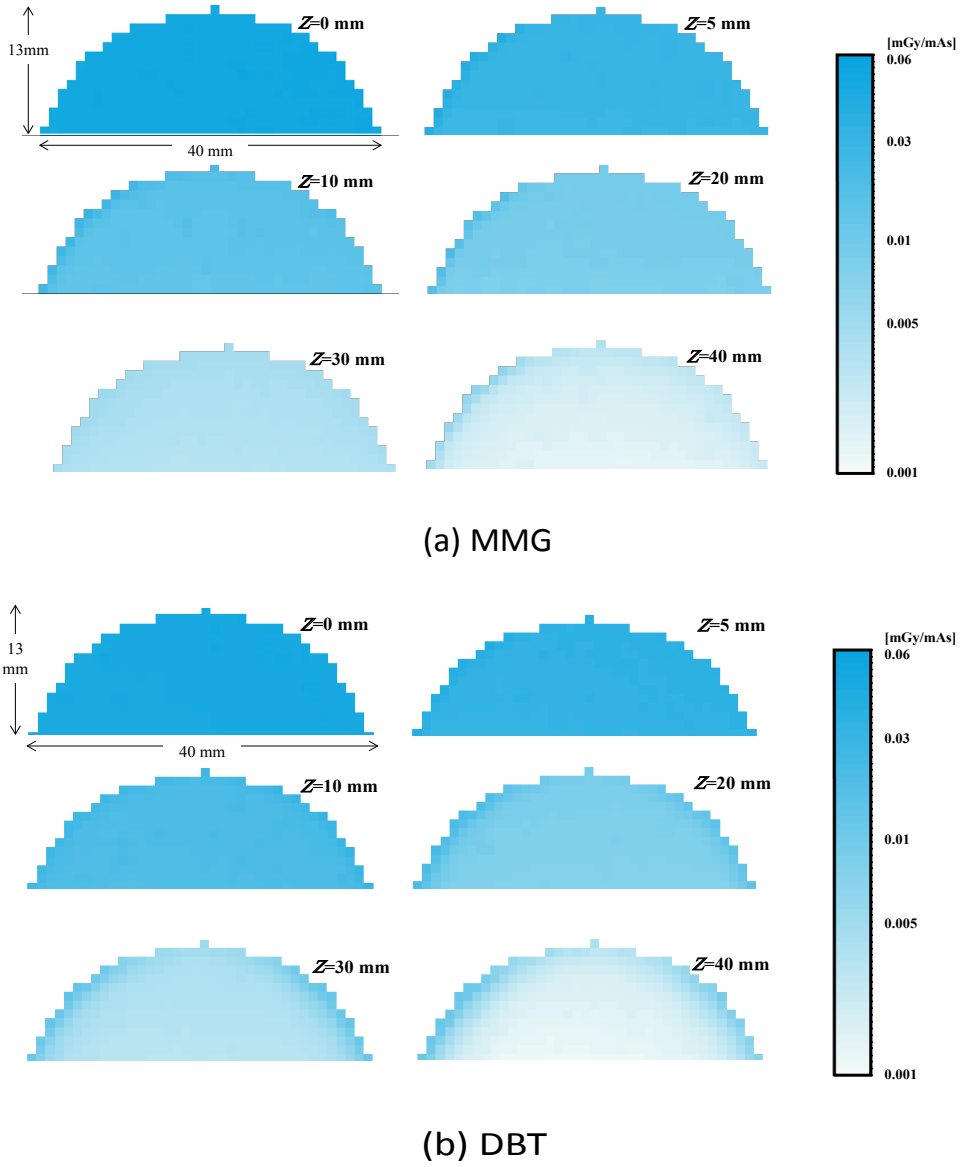

Figure 3. Color Maps of Absorbed dose D_d in Phantom in XY Direction (tube voltage 24 kV, φ40 mm). DBT, digital breast tomosynthesis; MMG, mean glandular dose

at the phantom edge was higher than that at a deep position in the phantom. This is because the oblique incidence of X-rays causes the primary X-rays to be incident on the sides of the phantom and the increased contribution of scattered radiation from the breast support increases the dose of the phantom. Previous studies have shown that DBT is associated with a higher edge dose than MMG, and our results corroborate this finding (Diaz et al., 2019).

Table 1 shows that $\bar{D}_{all}$ increased with an increase in the energy of both MMG and DBT regardless of the phantom size. This result is consistent with the previous ones because the coefficients factors g and c used for calculating MGD also increase with an increase in the energy (Dance et al., 2009).

Regarding the phantom size, $\bar{D}_{all}$ of MMG decreased with a decrease in the phantom size. This can be explained as follows: when the phantom size is small, the decrease in the scattered dose in the phantom contributes more than the increase in the scattered radiation from the breast support. In contrast, $\bar{D}_{all}$ of DBT was larger in the φ40-mm phantom at a tube voltage of 24 kV than in the φ160-mm phantom. This can be explained by the fact that the rate of increase in the scattered radiation from the breast support is larger than the rate of decrease in the scattered dose in the phantom because of the oblique incidence of X-rays.

The coefficient factor T for converting MGD of MMG to MGD of DBT reported by Dance et al., (2011) is 0.990 at a PMMA phantom thickness of 40 mm. As shown in Table 2, the R_T values measured using RCF were 0.985, 1.008, and 0.963 at tube voltages of 24, 28, and 32 kV, respectively. The average value was 0.985. These values are the same as those reported by Dance et al., (2011). Furthermore, the averages for φ80 mm and φ40 mm were 1.005 and 1.098, respectively. A smaller phantom size resulted in a larger R_T. This can be explained as follows: when the phantom size decreases, X-rays are obliquely incident on DBT and, therefore, the primary X-rays are incident on the side surface of the phantom, and the dose in

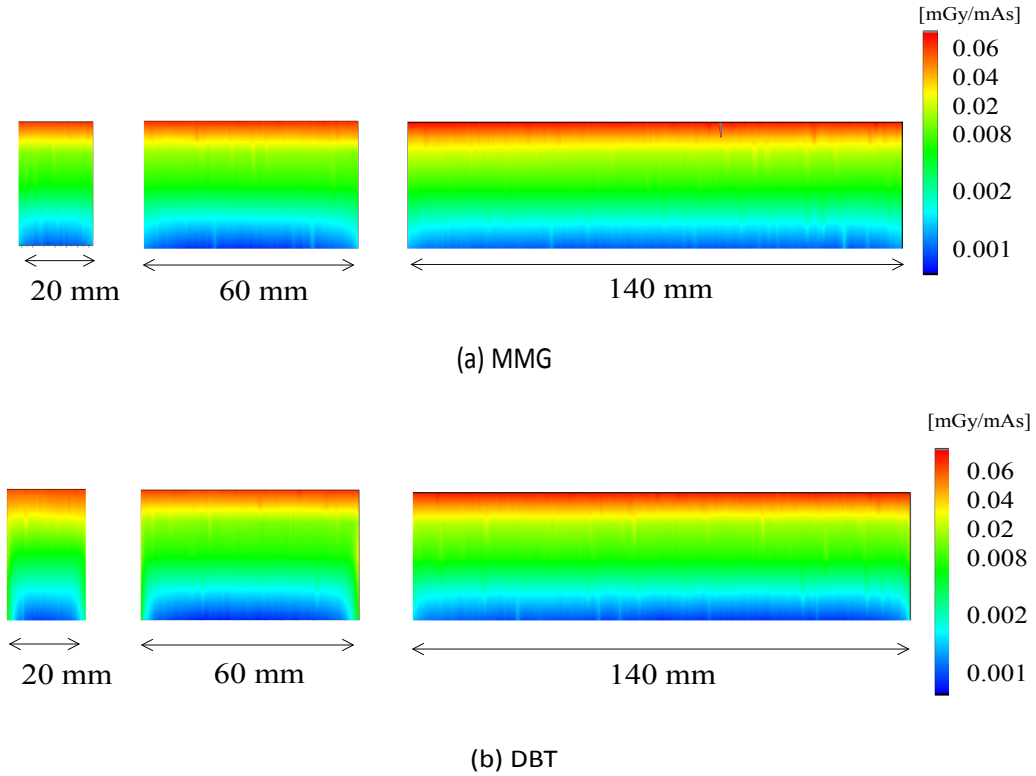

Figure 4. Color Map of D_d by the Depth to Differences in Phantom Size in the XZ Direction. (tube voltage, 24 kV). It presents at Y=10 mm position.

the phantom increases due to the contribution of scattered rays from the breast support. These are consistent with previous studies reporting the use of higher doses at the edge of the phantom when the angle increased (Flores et al., 2019). In addition, there is no contradiction with a previous report, which stated that the dose distribution at the depth Z of 10 mm was higher in the peripheral area owing to the effect of oblique incidence even in the absence of a compression plate (Fedon et al., 2018).

As shown in Figure 5, f_{40} and f_{80} values of MMG and DBT were <1 at most tube voltages and phantom sizes. Especially, the φ160-mm phantoms currently used for dose evaluation overestimate these values for subjects with small breast sizes. However, f_{40} at a tube voltage of 24 kV is 1.08, which is underestimated at the phantom size of φ160 mm. The risk assessment for breast cancer screening is assessed by stochastic effects. The cancer mortality rate due to radiation exposure is estimated by multiplying the effective dose by the lifetime risk factor according to the age at the time of exposure. If the MGD is 2 mGy/exposure with MMG, the lifetime fatal carcinogenic risk is 0.0006% by ICRP (ICRP, 2007). Considering that this study found f_{40} to be 1.08, if the individual's breast size is φ40 mm, the lifetime fatal carcinogenic risk would be 0.000648%. Previous dose assessments revealed that six people/million would develop breast cancer and die

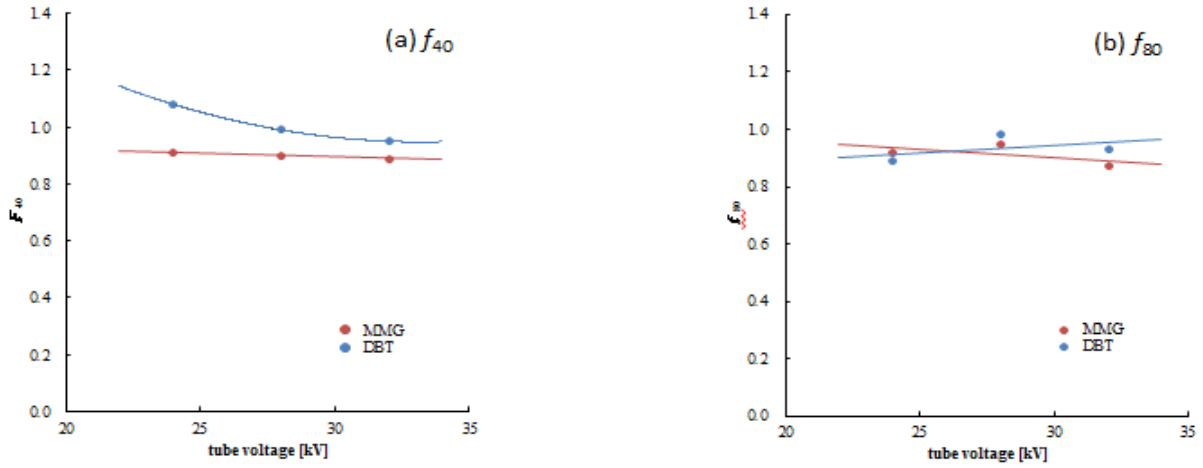

Figure 5. Ratio of D_{all} Difference by Phantom Size Based on the φ160 mm Phantom with Respect to DBT and MMG. DBT, digital breast tomosynthesis; MMG, mammography

because of DBT-based breast cancer screening; however, after taking the phantom size into account, 6.48 people/million were expected to die if the individual's breast size is φ40 mm. In the efficacy evaluation of DBT-based cancer screening, the risk of death owing to other factors is individually determined, the total value of these factors is compared with the life-saving effect of the screening, and a profit analysis is performed. Therefore, dose evaluation is one of the important factors that helps determine the effectiveness of breast cancer screening (Miglioretti et al., 2016).

Breast thickness was only 40 mm in this study. Also, the shape was evaluated only with a semi-cylindrical shape. In the future, it is necessary to change the phantom thickness, phantom size and phamtom shape in detail, in consideration of clinical conditions, in order to examine the correction method of MGD according to the phantom size more accurately. In the future, by applying this evaluation method to other DBT equipment and calculating correction values for each equipment, the geometric conditions of the breast can be incorporated as MGD correction coefficients for each equipment.

Author Contribution Statement

Erika Nakajima and Hitoshi Sato substantially contributed to the study conceptualization and to data analysis and interpretation. All authors critically reviewed and revised the manuscript draft and approved the final version for submission.

Acknowledgements

This article does not contain any studies with human participants.

Conflict of interest

No conflict of interest.

References

Alakhras M, Bourne R, Rickard M, et al (2013). Digital tomosynthesis: a new future for breast imaging?. *Clin Radiol*, **68**, 225-36.

Ali RM, Andrew E, Mark FM, et al (2015). A method for calculating effective lifetime risk of radiation-induced cancer from screening mammography. *Radiography*, **21**, 298-303.

Chong A, Weinstein SP, McDonald ES, et al (2019). Digital breast tomosynthesis: concepts and clinical practice. *Radiology*, **292**, 1-14.

Dance DR (1990). Monte Carlo calculation of conversion factors for the estimation of mean glandular breast dose. *Phys Med Biol*, **35**, 1211-9.

Dance DR, Hunt RA, Bakic PR, et al (2005). Breast dosimetry using high-resolution voxel phantoms. *Radiat Prot Dosimetry*, **14**, 359-63.

Dance DR, Young KC, van Engen RE (2009). Further factors for the estimation of mean glandular dose using the United Kingdom, European and IAEA breast dosimetry protocols. *Phys Med Biol*, **54**, 4361-72.

Dance DR, Young KC, van Engen RE (2011). Estimation of mean glandular dose for breast tomosynthesis: factors for use with the UK, European and IAEA breast dosimetry protocols. *Phys Med Biol*, **56**, 453-71.

Chang TY, Lai KJ, Tu CY, et al (2020). Three-layer heterogeneous mammographic phantoms for Monte Carlo simulation of normalized glandular dose coefficients in mammography. *Sci Rep*, **10**, 1-10.

Diaz O, Elangovan P, Young KC, et al (2019). Simple method for computing scattered radiation in breast tomosynthesis. *Med Phys*, **46**, 4826-36.

Fedon C, Caballo M, Sechopoulos I (2018). Internal breast dosimetry in mammography: Monte Carlo validation in homogeneous and anthropomorphic breast phantoms with a clinical mammography system. *Med Phys*, **45**, 3950-61.

Flores MB, Mourão AP, Oliveira FA, et al (2019). Dose profile evaluation in digital breast tomosynthesis exposition using radiochromic film. *Appl Radiat Isot*, **152**, 140-4.

Gilbert FJ, Tucker L, Gillan MG, et al (2015). The TOMMY trial: a comparison of TOMosynthesis with digital MammographY in the UK NHS Breast Screening Programme--a multicentre retrospective reading study comparing the diagnostic performance of digital breast tomosynthesis and digital mammography with digital mammography alone. *Health Technol Assess*, **19**, 1-136.

Helvie MA (2010). Digital mammography imaging: breast tomosynthesis and advanced applications. *Radiol Clin North Am*, **48**, 917-29.

Hernandez AM, Seibert JA, Boone JM (2015). Breast dose in mammography is about 30% lower when realistic heterogeneous glandular distributions are considered. *Med Phys*, **42**, 6337-48.

Houssami N, Skaane P (2013). Overview of the evidence on digital breast tomosynthesis in breast cancer detection. *Breast J*, **22**, 101-8.

Huda A, Antar A (2020). Evaluation of radiation dose for patients undergoing mammography in Qatar. *Radiat Prot Dosim*, **189**, 354-61.

ICRP (2007). The 2007 recommendations of the International Commission on Radiological Protection. ICRP Publication 103. Ann ICRP 37.

Kulkarni S, Freitas V, Muradali D (2021). Digital breast tomosynthesis: potential benefits in routine clinical practice. *Can Assoc Radiol J*, **73**, 107-20.

Mackenzie A, Thomson EL, Mitchell M, et al (2021). Virtual clinical trial to compare cancer detection using combinations of 2D mammography, digital breast tomosynthesis and synthetic 2D imaging. *Eur Radiol*, **32**, 806-14.

Miglioretti DL, Lange J, van den Broek JJ, et al (2016). Radiation-induced breast cancer incidence and mortality from digital mammography screening: a modeling study. *Ann Intern Med*, **164**, 205-14.

National Institute of Bioscience and Human-Technology (1996). Human body dimensions data for ergonomic design. Osaka (Japan): The Institute 219. in Japanese.

Sarno A, Masi M, Antonelli N, et al (2017). Dose volume distribution in digital breast tomosynthesis: a phantom study. *Radiat Plasma Med Sci*, **1**, 322-8.

Sarno A, Mettivier G, Di Lillo F, et al (2018). Homogeneous vs. patient specific breast models for Monte Carlo evaluation of mean glandular dose in mammography. *Physica Medica*, **51**, 56-63.

Sarno A, Mettivier G, Di Lillo F, et al (2018). Normalized glandular dose coefficients in mammography, digital breast tomosynthesis and dedicated breast CT. *Physica Medica*, **55**, 142-8.

Saur S, Frengen J (2008). GafChromic EBT film dosimetry with flatbed CCD scanner: a novel background correction method and full dose uncertainty analysis. *Med Phys*, **35**, 3094-101.

Sechopoulos I, Bliznakova K, Qin X, et al (2012). Characterization

of the homogeneous tissue mixture approximation in breast imaging dosimetry. *Med Phys*, **39**, 5050-9.
Sechopoulos I (2013). A review of breast tomosynthesis. Part I. The image acquisition process. *Med Phys*, **40**, 014301.
Skaane P, Bandos AI, Gullien R, et al (2013). Comparison of digital mammography alone and digital mammography plus tomosynthesis in a population-based screening program. *Radiology*, **267**, 47-56.
Suzuki A, Ishida T, Watanabe G, et al (2021). Aiming for the best screening method. *J Jpn Assoc Breast Cancer Screen*, **30**, 11-4. in Japanese.
Sylvia H.H, Astrid H, Stefan S (2011). Advantages and disadvantages of mammography. *Breast Care*, **6**, 199–207.
Thomas MK, Jacob L, Jeffrey HN (2002). Comparison of the performance of screening mammography, physical examination, and breast US and evaluation of factors that influence them: an analysis of 27,825 patient evaluations. *Radiology*, **225**, 165-75.
Uematsu T (2013). The emerging role of breast tomosynthesis. *Breast Cancer*, **20**, 204-12.
Wang W, Qiu R, Ren L, et al (2017). Monte Carlo calculation of conversion coefficients for dose estimation in mammography based on a 3D detailed breast model. *Med Phys*, **44**, 2503-14.